ON THE SPECTRA LUMINESCENCE EMISSION OF NATURAL COAL AND GRAPHITE SPECIMENS

Irena Kostova[a], Laura Tormo[b], Elena Crespo-Feo[c], Javier Garcia-Guinea[b],

[a]Sofia University "St Kliment Ohridski", Department of Geology and Paleontology, Sofia 1000, Bulgaria
[b]Museo Nacional Ciencias Naturales, CSIC. C/José Gutiérrez Abascal 2. Madrid 28006, Spain.
[c]Facultad de Ciencias Geologicas. C/Antonio Novais 2. Madrid 28040, Spain.
Author for Correspondence: irenko@gea.uni-sofia.bg

ABSTRACT

The little luminescence shown by coals has been attributed to accessorial minerals and poly-nuclear aromatic hydrocarbons, such as exinite, vitrinite or inertinite, while the luminescence quenching has been found in coal-hydrogenation asphaltenes and pyridine extracts. Nowadays, the spatial resolution and the improved luminescence efficiency of the modern spectrometers allow explain some details on the luminescent emission centers in the same theoretical frame. Accordingly, we selected Museum historical coals specimens with different rank, i.e., peat, lignite, sub-bituminous, bituminous, anthracite, to be analyzed by the spectra cathodoluminescence probe (CL) of an environmental scanning electron microscopy (ESEM) with an energy dispersive spectrometry analyzer (EDS). Additional analytical controls were also performed by X-ray diffraction (XRD), X-ray fluorescence (XRF) and Raman spectrometries. We conclude that coals may display different luminescence emission features from several sources, as follows: (i) broad band of intense luminescence from poly-nuclear aromatic hydrocarbons, (ii) little visible broadband luminescence attributed to band-tail states caused by variations in the energy gap of individual sp^2 carbon clusters due to their difference in size and/or shape, (iii) silicate impurities as responsible of the common luminescence peak at 325nm observed in coals attributed to non-bridging oxygen hole centres (≡ Si–O•) probably generated from precursor Si–O–C species formed by ≡ Si–O• defects and carbon atoms; (iv) a 710 nm CL emission commonly detected also in wood and ivories which has been correlated with hydrocarbon groups of chlorophyll or lignine. Coals are very complex rocks composed by both organic and inorganic phases with variable and complex spectra needing more analyses together with carbonous standards of graphite, silicon carbide, stuffed carbon silica and diamond at variable experimental conditions.

Keywords: *Luminescence, Cathodoluminescence, Raman, NBOHC, Coal, Graphite,*

INTRODUCTION

The increasing use of the Spectra Cathodoluminescence (CL) and X-ray Energy Dispersive Spectroscopy (EDS) probes coupled to environmental electron microscopes (ESEM) for geological materials analyses suggest us to enquire on the frequent observed spectra CL of nominally non-luminescent natural carbonous compounds such as graphite and coals. The new devices such as the MONOCL3 Gatam probe records CL spectra at high resolution by a retractable parabolic diamond mirror and

photomultiplier tube which collect and amplify the CL emission with great quantum efficiency. These new spatially-resolved facilities could provide accurate spectral details not previously observed in non-luminescent materials. Accordingly, it seems important to clarify feasible causes of CL emissions in these carbonous compounds exhibiting low luminescence. From the sixties decade it is well known that the little visible luminescence shown by coals, if any, come up from accessorial minerals in coals such as feldspar, quartz, calcite, gypsum and kaolinite. In addition, coals with large amounts of poly-nuclear aromatic hydrocarbons (PAH) as well as large amounts of free radicals should exhibit an appreciable visible luminescence (1). The lack of luminescence in solid coals or solid derivatives, such as coal-hydrogenation asphaltenes and pyridine extracts, could be explained by quenching due to various factors. Carbon-disulphide extracts of coal macerals, e.g., exinite, vitrinite, inertinite, exhibit luminescence emission which can be employed to identify individual polycyclic hydrocarbons (2). Recently, many other natural hydrocarbons and resins associated to coals, slates or peatified woods, e.g. such as hatchettite, fichtelite, hartite, ozokerite are being studied by spectroscopy, since they exhibit very different and complex Raman spectra (3,4). Early comparative studies on the Raman and Luminescence spectra in coal and graphite show large similarities among coal and disordered graphite suggesting that the Raman peak near 1600 cm^{-1} originates from the zone-center E_{2g} mode of graphite and the assignment of the peak around 1370 cm^{-1} for disordered graphite as the A_{1g} mode of D_{6h} (5). The Raman spectra consist of two main bands at 1600 and 1360 cm^{-1} which usually have bandwidths at half peak intensity depending on the rank of the coal. The origin of these bands is best discussed in relation to those found in graphites and carbons. The band at 1600 cm^{-1} has been interpreted as being related to the 1580 cm^{-1} band of graphite which has been assigned to the E_{2g} carbon-carbon in-plane stretching vibration. The Raman band at 1360 cm^{-1} has been attributed to defects present in structural units and disorder (6). Water and hydroxyl groups commonly integrated in coals and associated clay minerals must be considered analyzing dehydration induced luminescence, e.g., thermoluminescence (TL) or CL. Both techniques produce tribo-luminescence phenomena during the luminescence measurements, i.e., extensive mechanical distortion produced on freezing and drying in a wet/dry cycled reaction sequence (7,8). Water and coupled hydro-silicate molecules could be involved in the thermal stimulation processes to obtain luminescence emission from natural coals. An intense ultraviolet and green photoluminescence can be observed from sol–gel derived silica containing hydrogenated carbon (9). The intensity of the UV PL 330 nm emission increases significantly with the increase of OH groups adsorbed on the surface of porous silica since strain Si–O bonds creating silicon vacancy-hole centers, Si–O bonding defects seem to be responsible of the NBOHC, non-bridging oxygen hole centres ≡ Si –O•) for the 340nm emission (10). Concerning silica in coals, detritic and diagenetic quartz and amorphous silica phases are frequently found in natural coals (11); the integrated SEM-cathodoluminescence systems are being used to classify quartz grains in coals on the basis of their origin, i.e., metamorphic, igneous, hydrothermal (12) but these spectra UV luminescence bands are commonly overlooked. Diamond and graphite carbon—carbon structures show different characteristic luminescence broad bands, observed for diamonds peaked ca 617 nm due to electron-lattice interaction of the nitrogen centers (13). Graphites show signs of a perceptible broadband luminescence explained by band-tail states produced by changes in the energy gap of individual sp^2 carbon clusters by

differences in size and/or shape (14). This paper focuses on the luminescence emissions of carbonous compounds studied by EDS, ESEM XRF, and CL. For comparison, we also perform Raman spectroscopy as a consolidated technique used to check metamorphism and maturation grade of coals (15).

MATERIALS AND EXPERIMENTAL METHODS

We select aliquots of 9 historical-international coals kept in the reserve of the MNCN museum (Madrid, Spain) with the following data-labeling: A2 Hartite ($C_{20}H_{34}$) from Gloggnitz (Vienne, Austria), A3 Lignite from Vienne, GB1 Coal from Cardiff (UK), GB3 Elaterite (Bitumen) from Derbyshire (UK), CS2 Lignite from Bohemia (Czec Rep.), NL1 Peat from Amsterdam, SU1 Shungite (C_{60}) from Olensk, Gon, Russia, USA1 Anthracite from Pennsylvania, TR1 Anthracite from Armenia (Turkey). In addition, we also select standards of graphite from Sri Lanka, black SiC with graphite, green SiC of Navarro S.A. and synthetic diamond Nanyang Zhongnan Diamond Co. of China. Some aliquots were pre-heated at different time-temperature sets from 100ºC to 600ºC in both, oxidant-atmospheric and reductor environments. In the graphite aliquots case, different crystallographic orientations (010) and (001) were also prepared for the luminescence measurements. Qualitative, quantitative and micro-textural XRD analyses of powdered coal aliquots were performed using XPOWDER software which also allows a full duplex control of the Philips PW-1710/00 diffractometer using the CuKα radiation with a Ni filter and a setting of 40kV and 40mA. The qualitative search-matching procedure was based on the ICDD-PDF2 database and the DIFDATA free database of the RRUFF Project. We utilize Boolean searching and chemical restraints to the initial elements previously detected by X-ray fluorescence spectrometry. Chemical XRF analyses of coals were performed in a Magic Philips X-ray fluorescence spectrometer operating an ultra-thin window and rhodium anode X-ray tube at 2.4 kW. The equipment has two coupled flux and sparkling detectors in the spectrometric chamber. In addition, there are three collimators of 150, 300 and 700µm for high resolution, quantitative analysis, and light elements analysis. Five analyser crystals, LiF 220, LiF 200, Ge, PE and Px1, allow the detection of all the usual chemical elements from oxygen to uranium. The coal powder pellets (trace elements) were mounted using 8.0 g of sample and 3.5 ml of elvacite with 20% acetone all together pressed at 200 KNcm^{-2}. The ESEM XL30 microscope of FEI Company is a facility sited in the MNCN Museum. It is a low-vacuum ESEM which enables high-resolution inspection and chemical analysis of non-conductive specimens. The ESEM microscope in low vacuum mode admits hydrated samples to be studied in their original state with the Large Field Detector (LFD), since it is close to the sample to avoid electron losses. This ESEM can also work at high vacuum conditions with samples covered with sputtered gold providing a better resolution in electronic images and more accurate chemical analyses by EDS. The ESEM resolution at high vacuum was at 3.0nm at 30kV (SE), 10nm at 3kV (SE) and 4.0nm at 30kV (BSE), while operating at low-vacuum it was at 3.0nm at 30kV (SE), 4.0nm at 30kV (BSE) and < 12nm at 3kV (SE). The accelerating voltage was at 200V – 30kV and the probe current up to 2µA continuously adjustable. The ESEM detectors are as follows: the LFD, Everhardt-Thornley or High-vacuum Secondary Electrons Detector (SED), the IR-CCD camera, a solid-state BSE detector and a new gaseous analytical electron detector (GAD). The organic oxygen concentrations were also calculated from the observed oxygen intensities using the "ZAF" program to correct atomic number, absorption and fluorescence effects in the coal matrix. In addition, this

SEM has a new coupled MONOCL3 Gatan probe to record CL spectra and panchromatic and monochromatic plots with a PA-3 photomultiplier attached to the ESEM. The PMT covers a spectral range of 185nm to 850nm, and is most sensitive in the blue parts of the spectrum. A retractable parabolic diamond mirror and a photomultiplier tube are used to collect and amplify luminescence. The sample was positioned 16.2 mm beneath the bottom of the CL mirror assembly. The excitation for CL measurements was provided at 25 kV electron beam. Coal sliced sample-aliquots were polished for both ESEM-EDS and micro-Raman plane measurements. The micro-Raman spectroscopy study was performed by single spectra and hyperspectral line-scans using a new Thermo Fischer DXR Raman Microscope (West Palm Beach, FL 33407, USA), which has point-and-shoot Raman capability of one micron spatial resolution. We select the 20X objective of the confocal microscope together with a laser source 532 nm at 6 mW in mode laser power at 100%. The average spectral resolution in the Raman shift ranging from 100 to 3600 cm-1 was 4 cm^{-1}, i.e., grating 900 lines / mm and spot size 2 µm. The system was operated under OMNIC 1.0 software fitting working conditions such as pinhole aperture of 25 µm, bleaching time 30 s; four exposures average timed 10 s each. For the Raman quantification of spectral curves is necessary to derive consistent spectral parameters assuming that for pre-graphitic and graphitic natural organic matter (NOM), Raman spectra exhibit no fluorescence background and baseline subtraction is simple. For less mature materials, the fluorescence background is considerable and the fluorescence intensity augments as maturity decreases. Raman spectra are generally broad and the wings of the bands can easily be confused with the fluorescence background. The number and spectral profiles of components used in the fitting procedure has been addressed by many authors on synthetic and natural carbonaceous materials (15). Different fitting procedures have been proposed with respect to the number of components (from 1 to 4) and spectral profiles (Lorentzian, Voigt, Gaussian, etc.). The G-band in a perfect single crystal of graphite can be definitely allocated to the E_{2g2} vibration mode and completely fitted with a Lorentzian profile; conversely the other "Disordered" components are induced by defects in the crystal lattice with difficult understanding and fitting procedures. Here we used Lorentz functions by the χ^2 criterion to build spectral parameters sensitive to the maturity of the samples. The fitting was performed with ORIGIN v.8 software obtaining spectral parameters derived for each spectrum, as follows: (i) spectral peak position ωD,G, (ii) peak intensity ID,G, (iii) integrated intensity AD,G and the full width at half maximum FWHM—D—G.

RESULTS

Mineral phases by XRD.- The obtained XRD profiles of powdered coal aliquot samples (Figure 1) were studied by XPOWDER software performing background subtraction, Kα2 stripping and chemical elements restraining. In addition to the predicted amorphous broad XRD bands characteristic in coals, the Boolean search-matching on the ICDD-PDF2 and RRUFF databases suggest us the following PDF2 card files: (sample A2) Broad band peaked at circa 18º 2θ and the Chaoite $C_{20}H_{34}$ card file 22-1069 roughly matched by the Xpowder software; (sample A3) A similar broad XRD band with two maxima peaks at 18º and 23º 2θ in which the program propose the card 22-0586 Calcite; (sample GB1) A broad band of amorphous coal peaked at 27º 2θ and the following proposed card-files: 18-1170 opal-CT, 18-0948 Illite, 18-2392

aragonite (authigenic) and 18-0710, pyrite; (sample GB3) A broad band of amorphous bitumen peaked at circa 18º θ2 with suggested card s 22-1069 chaoite and 22-0710 pyrite; (sample CS2) amorphous XRD band with recommended cards 83-2284 native sulfur and 83-0710 pyrite; (sample NL1) an amorphous looking XRD spectrum and many accessorial minerals such as: 73-0335 tridymite and 73-1161 quartz corresponding to opal-CT and chert, 73-0248 sulfur, 73-0710 pyrite and 73-0586 calcite; (sample SU1) shungite with 77-0126 opal-CT, 77-0216 barite, 77-0586 calcite and 77-0710 pyrite; (sample USA1) anthracite 76-0217 barite, 76-1306 illite, 76-0586 calcite, 76-0710 pyrite, 76-0592 galena, 76-0164 kaolinite; and for the sample TR1 anthracite specimen the Xpowder software suggests 06-0710 Pyrite, 06-0586 Calcite, 06-1161 Quartz, 06-0242 Opal CT, 06-0263 Illite.

Chemical analyses by XRF and ESEM-EDS.- Tables 1a&b show the chemical analyses of the major elements performed on coal specimens and table 2 the trace elements of the same samples. Sample A2, under EDS exhibits carbon maxima % amounts of C_{85} (O_{15}) together with accessorial Ca and Fe, i.e., $CaCO_3$ and FeS_2 the XRF analyses support this result and displays additional 1107 ppm of Ba, 139 ppm of Ni and 105 ppm of Th. Sample A3, under EDS, shows carbon maxima % amounts of C_{66} ($O_{17}Si_{16}$) and accessorial traces of Pb, S, Cl, Mg, Fe, e.g, calcite, pyrite, silica, etc., by XRF can also be detected accessorial Zr and P; the ESEM image shows well-preserved wood structures (Figure 2a) Sample GB1, by EDS, displays areas with maxima % amounts of C_{81} (O_{17}) and C_{73} (O_{26}); other EDS analyses such as $C_{26}O_{52}Al_{11}Si_{10}$ suggest kaolinite impurities, pyrite (Figure 2b) and caolinite-calcite mixtures, e.g., $C_{26}O_{57}Al_4Si_7Ca_3$. The XRF data give also accessorial Mn, Ti,P, Ba, Sr, Zr, V and Cs (Tables 1&2). Sample GB3, by EDS, confirms to have areas with $C_{84}O_{15}S_1$ and accessorial SiO_2 and $CaCO_3$, the XRF analyses show also traces of Sr, Ba, V, La, Zn, Pb and Cl which agree with several mineral phases (Figure 2c) Sample CS1, under EDS, shows $C_{30}O_{60}S_5$ and minor amounts of Al, K, Ca and Fe which could be attributed to the presence of claystone illite. The XRF analyses confirm accessorial amounts of Fe, Ca, Al, Ba, V, Cl. Sample NL1 display maxima EDS carbon contents of C_{67} (O_{31}) or C_{70} ($O_{29}Si_1$), many heavy metal spots, e.g., spot analysis $C_{35}O_{24}Si_{20}Ti_6V_6Fe_5Ni_1Zr_2$. and calcium carbonate areas. The XRF spectrometry confirms also Ba, Zr, V, La, P, Ti, Cl, Mn, Al and abundant calcium (5.3%). Sample SU1, by EDS, exhibits maxima %C of $C_{87}O_{11}$ with accessorial S, Cl and Si, other ESEM spots display Fe, Ni, Cu, V. By XRF we confirm important total amounts of CaO (~12%), Fe_2O_3 (~8%), SiO_2 (~3%), P_2O_5 (~3%), Na_2O (~1%) and TiO_2 (~1%). Sample USA1 display EDS spots up to $C_{88}O_{10}Si_1$ with accessorial S, K, Ti, i.e., minor amounts of illite and pyrite, other EDS spots show $C_{75}O_{18}Al_3Si_3$, i.e., with some kaolinite. Concerning the XRF data it is interesting to note the 252 ppm of Sr, 219 ppm of Ba and the 79 ppm of Zn. Sample TR1, by EDS, reach up clean spots of $C_{90}O_8S_1$, other as $C_{70}O_{19}Al_5Si_6$, i.e., with accessorial kaolinite. It also has minor S, Fe, K, Na, Mg by EDS. Under XRD we also detect S, Cl, Zr.

Raman spectra on carbonous regions in coals

Raman spectroscopy was employed for determining the maturity of the NOM of the nine coals since it presents the following advantages: (i) fast measurements at a micrometric scale requiring small amount of material; (ii) it does not require chemical-mechanical pre-treatments, (iii) it make available abiogenic spectral tracers mostly

helpful for meteoritic studies. The excitation wavelength was 532 nm since it provides better results than the red laser sources obtaining G and D Raman bands. The most responsive spectral NOM maturity tracers are the width of the D-band (FWHM-D), the ratio of the peak intensities of the D- and G-bands (I_D/I_G), the normalized ratio of the band integrated intensities $A_D/[A_D + A_G]$ and the width of the G-band (FWHM-G) (15). These parameters are considered under caution since for poorly ordered carbonaceous materials the archetypal determination of the coherent domain length (La) using ID/IG is not suitable. Hartite A2 and Lignite A3 from Vienne display highest Raman emissions beyond the 25.000 a.u. and similar spectral positions circa ωD 1347 and ωG 1570 cm^{-1} (Figure 3). Parameter I_D/I_G values in both coal specimens are 0.819 and 0.660 since G-band and graphitic features are taller in respect to D-band. Similar shape and parameters exhibits the Lignite CS2 from Bohemia (Figure 4) and the Welsh coals from Cardiff emitting Raman signal at low intensity, i.e.,10.000 a.u. Furthermore, anthracites USA1 from Pennsylvania and TR1 from Armenia display very different Raman spectra with a detached G-band unambiguously assigned to the E_{2g2} vibration mode and perfectly fitted with the Lorentzian profile conversely their D-bands appear clearly reduced. Very interesting is the mixed spectral structure of the Russian shungite SU1 exhibiting the following parameters: ωD 1292 cm^{-1}, ωG 1586 cm^{-1}, I_D/I_G 2.021, FWHM-D 104.52 cm^{-1}, FWHM-G 54.41 cm^{-1}, $A_D/[A_D+A_G]$ 0.797. (Figure 4 Table). The peat NL1 from Amsterdam displays a noisy Raman spectrum with invaluable information.

Spectra cathodoluminescence emission of carbonous rocks

A first look of the comparative plot of the coals spectra CL (Figure 5) shows the following remarkable features: (i) two spectra with a broad band of CL emission USA1 7000 a.u. and GB3 12000 a.u. while the remaining coals display less intense CL emissions, (ii) a 710 nm sharp CL peak from the less mature coals, such as the NL1 peat case at 12000 nm, (iii) a general sharp peak at ca 325 nm, (iv) variability of the broad band from the flat shape of the Russian shungite SU1 up to the big broad band of the GB3 peaked at ca 12000 a.u. The luminescence emission of natural coals stem from very different sources together with modifiers and/or quenchers, since they have accessorial minerals, e.g., feldspar, quartz, calcite, gypsum and kaolinite, and variable amounts of luminescence from poly-nuclear aromatic hydrocarbons and the CL emission quenching effect of other components, such as asphaltenes and pyridines. To explain these interesting features circumventing these varied problems we also record spectral CL from carbonous geochemical standards such as, extra-pure graphite from Sri Lanka oriented along with (001) and (010), graphitic black silicon carbide, pure green silicon carbide, synthetic transparent diamond and an inclusion of quartz found inside natural graphite. We also operate at different condition of low vacuum and high vacuum to be under control the humidity conditions of the ESEM-CL device. A first look of the comparative plot of the spectra CL of the carbonous standards non-coals (Figure 6) shows the following remarkable features: (i) graphite pure material does not show appreciable luminescence and/or sharp CL peaks in despite of different orientations and experimental conditions. Perhaps, operating at low vacuum on the (010) crystallographic orientation is possible to detect a little broad band peaked at circa 600 nm, (ii) this same broad band shifted to 580 nm is also observed in black SiC, i.e., graphite-rich carborundum being more intense in the pure green SiC, (iii) in the transparent-diamond case, the crystalline structure changes being a three-dimensional

network of covalent-bonded carbon atoms, exhibiting more spectral shift with a maximum ca 520 nm and stronger intensity (108 000 a.u.). (iv) a spectrum CL of quartz found inside natural graphite with strong UV-blue peak with maximum at 340 nm and a shoulder circa 325 nm.

DISCUSSION

From our results we confirm that the luminescence shown by coals stem from accessorial minerals and from poly-nuclear aromatic hydrocarbons as was described long time ago (1). This observed broad band of luminescence from poly-nuclear aromatic hydrocarbons is very different than those other observed in diamond and graphite carbon—carbon structures since it has been proved that: (i) Diamonds show a characteristic broadband luminescence observed from approximately 1.5 to 2.5 eV and centered at ~2 eV. The photo-luminescent transitions attributed to the zero-phonon lines of nitrogen centers observed at 1.945 and 2.154 eV., accordingly, this luminescent broadband could be due to electron-lattice interaction of the nitrogen centers (13); (ii) Graphite specimens can exhibit a visible broadband luminescence attributed to band-tail states caused by variations in the energy gap of individual sp^2 carbon clusters due to their difference in size and/or shape (14). Other components such as asphaltenes and pyridines could quench luminescence emissions (1). Concerning accessorial silicate impurities, they could be responsible of the general UV-blue 325 nm luminescence main emission of coals since coals has two important elements: silica and water-hydroxyl groups. Previously, we demonstrated (10) that the 340nm emission peak in the luminescence spectra of tectosilicate minerals, e.g., groups of silica, feldspars, feldspathoids, could be observed when the three-dimensional (3D)-framework silicon–oxygen lattices is stressed. The Si–O strained structures include some nonbridging oxygen or silicon vacancy-hole centers, and Si–O bonding defects which seem to be responsible for the 340nm emission. Using different luminescence techniques on different silicates such as quartz, hydrous-silica, feldspar, sodalite, etc, at different physic-chemical conditions we then concluded that for tectosilicate 3D lattices, a correlation between the 340nm luminescence emission band and stressed Si–O bonds exists. In the coals case, the Si–O strained structures can be achieved with surrounding hydroxyl groups linked to both, Si–O and C–O bonds. Here we analyze a spectrum CL of SiO_2, found inside natural graphite, exhibiting a strong UV-blue peak with maximum at 340 nm and a shoulder circa 325 nm. A similar 335 nm emission accompanied by a shoulder at 325 nm was observed in C-doped silica synthesized by a sol-gel process using tetraethoxysilane as the precursor and glucose as the carbon source, followed by thermal treatment at temperatures from 400 to 900º C in air and ambient N2 (9). These authors studied the intense ultraviolet and green room-temperature photoluminescence (PL) at 335, 370 and 500 nm explaining that the 335 emission is originated from non-bridging oxygen hole centres ≡ Si –O•) and the 370 nm emission correlates with Si–O–C species formed by ≡ Si –O• defects and carbon atoms. The 370 nm emission may be associated with the Si-O-C species formed by drop Si-O defects and carbon atoms. Moreover they suggest that the 500 nm band results from hydrogenated carbon embedded in silica which mainly derived from the decomposition of glucose. Both the 370 and 500 nm PL emissions disappeared when the sample is heated above 600ºC in air, indicating oxidative decomposition of the light-emitting centers in the material. Here we detect 325 nm emissions in all the coals which have silicon but it is not the case of the pure graphite

and diamond analyzed by CL. The enigmatic red CL peak observed at 710 nm commonly detected in wood, ivory and coal materials, e.g., NL1, CS2 and A3, has been correlated with hydrocarbon groups existent in chlorophyll or lignine (16) but further work seems necessary to broad knowledge on these relationships.

CONCLUSIONS

Main conclusions of this work are that the coals luminescence stem from different sources: (i) the main broad band of intense luminescence from poly-nuclear aromatic hydrocarbons, (ii) the little visible broadband luminescence attributed to band-tail states caused by variations in the energy gap of individual sp^2 carbon clusters due to their difference in size and/or shape, (iii) silicate impurities seems responsible of the common luminescence peak observed in near all the coals circa 325nm being attributed to non-bridging oxygen hole centres≡(Si –O•) probably generated from precursor Si–O–C species formed by ≡ Si–O• defects and carbon atoms; (iv) a 710 nm CL emission probably correlated with hydrocarbon groups of chlorophyll or lignin and not well studied by spatially resolved CL under ESEM. Carbonous standards of graphite, silicon carbide, stuffed carbon silica and diamond are very good standards to help with the large complexity of the natural coals.

ACKNOLEDGEMENTS

We are grateful for the financial support of the Spanish DGICYT I+D+I for the Project CGL2010-17108 (subprogram BTE). Author Irena Kostova have the benefit of a European SYNTHESYS fellowship to visit analytical facilities of Raman and ESEM—CL in the MNCN (Madrid, Spain).

REFERENCES

(1) Friedel, R. A. and Gibson H. L. Infra-red Luminescence (Fluorescence) and Reflectance of Coals, Coal Derivatives and Graphite Nature 1966, 211, 404–405.

(2) Drake, J.A.G., Jones, D.W., Causey, B.S., Kirkbright. Shpol'skii luminescence spectroscopy of extracts of coal and coal-tar pitch, Fuel, 1978, 57, 663—666.

(3) Jehlicka, J., Edwards H.G.M., Villar, S.E.J., Pokorny, J. Raman spectroscopic study of amorphous and crystalline hydrocarbons from soils, peats and lignite. Spectrochimica Acta Part. A. 2005, A 61, 2390–2398.

(4) Jehlicka, J., Edwards H.G.M., Villar, S.E.J., Raman spectroscopy of natural accumulated paraffins from rocks: evenkite, ozokerite and hatchetine. Spectrochimica Acta Part A 68 (2007) 1143–1148

(5) Tsu, R., Gonzalez J.H., Hernandez, I, Luengo, C.A. Raman scattering and luminescence in coal and graphite. Sol. State Comm. 1977. 24, 809—812.

(6) Green, P.D., Johnson, C.A., Thomas K.M. Applications of laser Raman microprobe spectroscopy to the characterization of coals and cokes. Fuel, 1983, 62, 1013—1023.

(7) Coyne, L.M. .Lahav, N, . Lawless, J.G Dehydration-induced luminescence in clay minerals. Nature, 1981, 292, 819—821

(8) Hessley RK, Coyne L.M. Spontaneous luminescence of coal. Abstracts of Papers of the American Chemical Society, 1987, 41-Fuel.

(9) He H.P., Wang, Y.X., Tang, H.G. Intense ultraviolet and green photoluminescence from sol-gel derived silica containing hydrogenated carbon Journal of Physics-Condensed Matter 2002, 14(45), 11867-11874.

(10) Garcia-Guinea, J; Correcher, V; Sanchez-Munoz, L; Finch, AA; Hole, DE; Townsend, P.D. On the luminescence emission band at 340 nm of stressed tectosilicate lattices. Nuclear Instruments & Methods In Physics Research Section A-Accelerators Spectrometers Detectors And Associated Equipment. 2007, 580, 648—651.

(11) R. Sykes, J.K. Lindqvist. Diagenetic quartz and amorphous silica in New Zealand coals. Org. Geochem. 1993, 20, (6) 855--866,

(12) Bassett K., Ettmuller, F., Bernet, M. Provenance analysis of the Paparoa and Brunner Coal Measures using integrated SEM-cathodoluminescence and optical microscopy New Zealand Journal of Geology & Geophysics, 2006, (49), 241–254.

(13) Bergman L., McClure, M.T. Glass J.I., Nemanich R.J. The origin of the broadband luminescence and the effect of nitrogen doping on the optical properties of diamond films. J. Appl. Phys., 1994, 76 (5), 3020—3027.

(14) Zhang R.Q., Bertran E., Lee S.T. Size dependence of energy gaps in small carbon clusters: the origin of broadband luminescence. Diamond and Related Materials, 1998, 7, 1663–1668.

(15) Quirico, E., Rouzaud, J.N., Bonal, L., Montagnac, G. Maturation grade of coals as revealed by Raman spectroscopy: Progress and problems Spectrochimica Acta Part A-Molecular and Biomolecular Spectroscopy 1995. 61(10), 2368-2377.

(16) Min, M., Lee W.s., Kim, Y.H., Bucklin, R.A. Non-desdructive detection of nitrogen in Chinese cabbage leaves using VIS-NIR spectroscopy. Hortscience 2006, 41(1), 162-166.

FIGURE CAPTIONS

Figure 1.- X-ray diffraction of powdered historical coal specimens. Note the amorphous character of the coals and the differences among them.

Tables 1a & b.- Chemical analyses of the historical coal aliquots by X-ray fluorescence spectrometry: (a) Major elements (%) and (b) Trace elements (ppm).

Figure 2.- Pictures of coal specimens taken in the Environmental Scanning Electron Microscope: (a) Sample A3 Lignite from Vienne preserving the wood structure, (b) GB1

Coal from Cardiff (UK) as an euxinic environment forming euhedral pyrite crystals, (c) GB3 Elaterite (Bitumen) from Derbyshire (UK) with mineral phases such as quartz, pyrite and aragonite.

Figure 3.- Raman spectra of the historical coals including the intensities of the maxima peaks. Note as USA and TR are more graphitic, i.e., anthracites while the Vienne bitumens, i.e., A2 & A3 exhibit the strong CL emission band characteristic of poly-nuclear aromatic hydrocarbons.

Figure 4.- Raman spectral maturity tracers of the coal samples following the Quirico et al., (2005) method. Bottom: sample A2 Raman spectrum and the obtained parameters.

Figure 5.- Spectra cathodoluminescence plots of the coal samples. Note the 325 nm and 710nn peaks and the broad bands of the coals with of poly-nuclear aromatic hydrocarbons.

Figure 6.- Spectra cathodoluminescence plots of the carbonous standards. Note the little broad band peaked at circa 600 nm in graphite (010) shifting to 580 nm in green silicon carbide and the spectrum CL of quartz found in graphite exhibiting the peak 340 nm with a shoulder circa 325 nm.

455

456 Table 1

MAJOR ELEMENTS (%)	A-2 Natrite (Aus-tria)	A-3 Ligni-te (Aus-tria)	GB-1 Coal (Car-diff)	GB-4 Natural coke (New-castle)	USA-1 Anthra-cite (Pensilva nia)	CS-2 Lignite (Bohe-mia)	NL-1 Peat Amster-dam	SU-1 Shungite (Olensk, Russia)	TR-1 Anthr-cite Arme-nia
SiO_2	-	-	2,12	3,42	18,01	0,56	3,68	2,83	8,28
Al_2O_3	-	0,02	5,71	3,5	27,04	2,03	2,98	0,24	15,97
Fe_2O_3 (total)	0,06	0,18	11,41	1,83	2,68	5,91	0,67	7,78	2,43
MnO	0,02	0,02	0,04	0,24	0,09	0,06	0,17	0,24	0,2
MgO	-	-	-	-	-	-	-	-	-
CaO	0,14	1,48	2,42	26,54	7,33	1,63	5,32	11,08	7,27
Na_2O	-	-	-	2,55	-	-	-	0,71	-
K_2O	-	-	-	0,56	-	-	0,4	0,26	0,4
TiO_2	0,02	0,02	0,17	0,24	3,26	0,12	0,23	0,7	3,23
P_2O_5	-	0,02	0,13	0,08	5,54	0,02	0,13	2,83	0,4
P.C.	85,23	96,92	42,06	26,78	15,59	77,4	79,15	12,05	19,34
TOTAL	85,47	98,64	64,05	65,74	79,54	87,73	92,74	38,71	57,52

457

458

459

460

461

462 Table 2

TRACE ELEMENTS (ppm)	A-2 Natrite (Aus-tria)	A-3 Ligni-te (Aus-tria)	GB-1 Coal (Car-diff)	GB-4 Natural coke (New-castle)	USA-1 Anthra-cite (Pensilva nia)	CS-2 Lignite (Bohe-mia)	NL-1 Peat Amster-dam	SU-1 Shungite (Olensk, Russia)	TR-1 Anthr-cite Arme-nia
Zr	-	17	16	17	12	23	16	16	18
Y	21	-	-	-	-	-	-	-	-
Rb	-	3	-	4	-	3	-	-	-
Sr	11	-	31	22	252	12	1	1	1
Cu	-	-	5	-	1	-	-	-	-
Ni	139	1	12	9	11	1	1	2	3
Co	18	5	11	6	9	8	5	5	5
Ce	30	-	-	-	1	-	-	-	-
Ba	1107	6	104	41	219	49	82	82	3
Cr	1	-	1	-	17	-	1	1	-
V	21	2	39	47	87	37	4	3	13
Th	105	-	-	-	-	-	-	-	-
Nb	32	2	3	3	1	6	3	4	2
La	17	-	5	8	32	1	4	3	9
Zn	60	-	-	559	79	-	-	-	-
Cs	26	13	37	9	40	12	33	33	4
Pb	11	-	6	786	5	-	-	-	-
Mo	21	-	-	-	-	-	-	-	-
F	-	-	-	-	46	-	-	-	-
S	11251	3426	34535	34477	18312	52293	8701	8701	8402
Cl	203	105	362	13207	184	80	345	345	167
Br	42	36	62	258	38	32	44	44	35

463

464

465

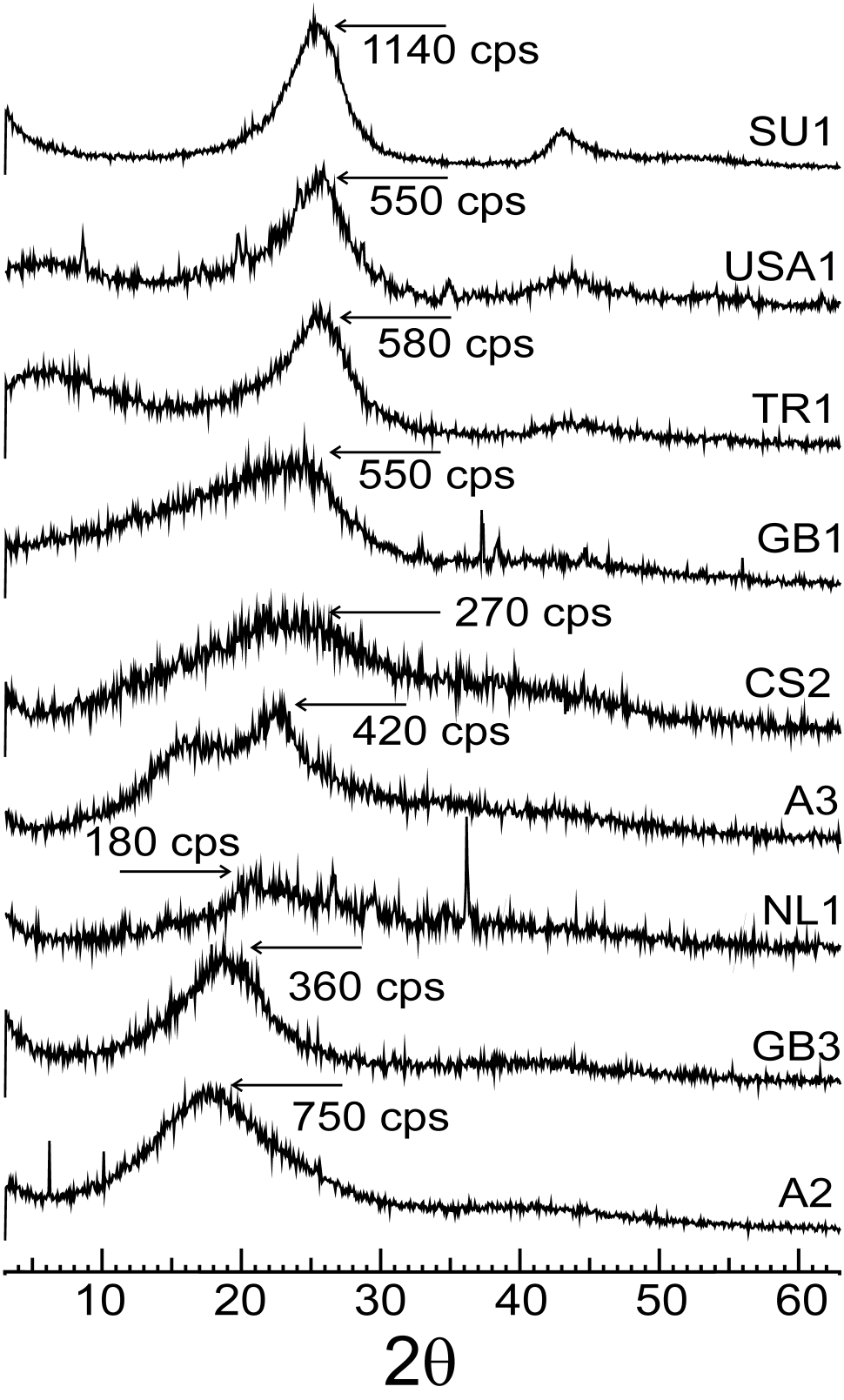
1140 cps
SU1
550 cps
USA1
580 cps
TR1
550 cps
GB1
270 cps
CS2
420 cps
A3
180 cps
NL1
360 cps
GB3
750 cps
A2
10
20
30
40
50
60
2θ

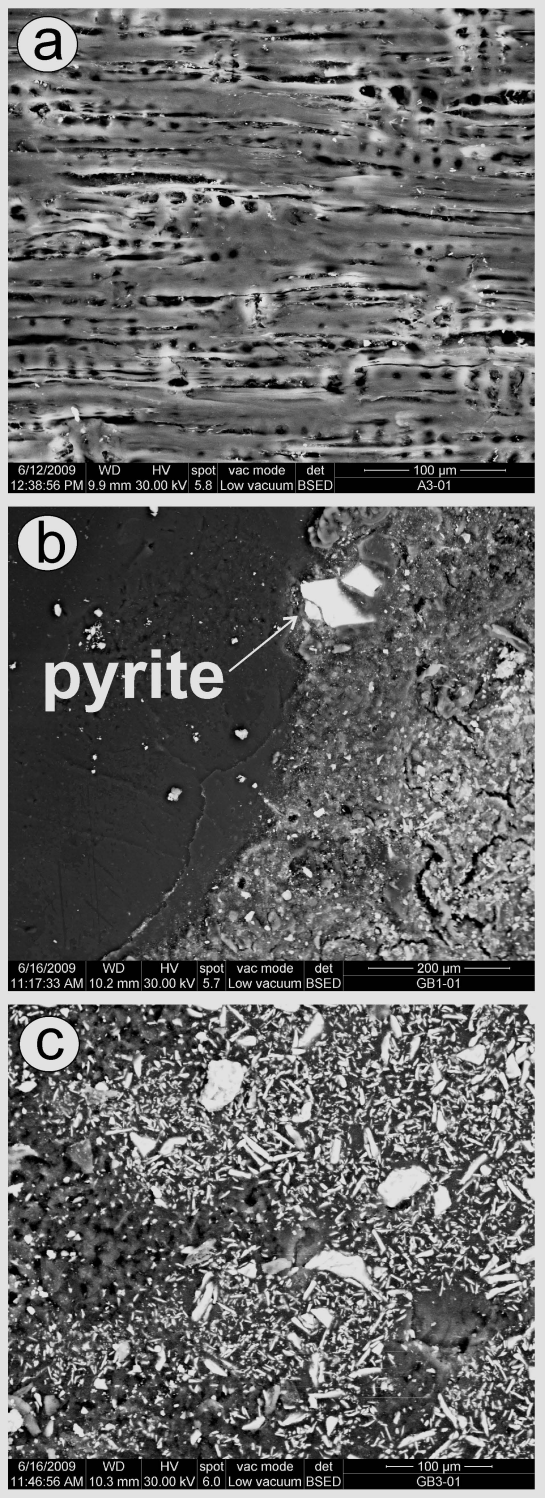
a
6/12/2009 WD HV spot vac mode det 100 µm
12:38:56 PM 9.9 mm 30.00 kV 5.8 Low vacuum BSED A3-01
b
pyrite
6/16/2009 WD HV spot vac mode det 200 µm
11:17:33 AM 10.2 mm 30.00 kV 5.7 Low vacuum BSED GB1-01
c
6/16/2009 WD HV spot vac mode det 100 µm
11:46:56 AM 10.3 mm 30.00 kV 6.0 Low vacuum BSED GB3-01

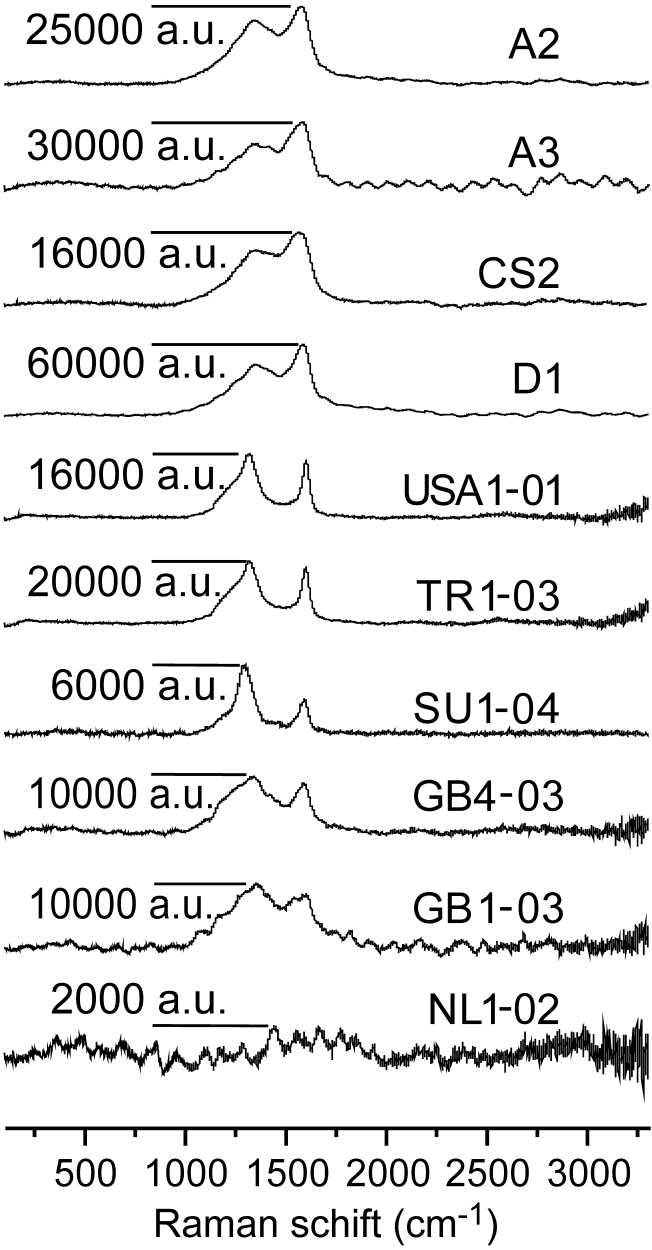
25000 a.u.
A2
30000 a.u.
A3
16000 a.u.
CS2
60000 a.u.
D1
16000 a.u.
USA1-01
20000 a.u.
TR1-03
6000 a.u.
SU1-04
10000 a.u.
GB4-03
10000 a.u.
GB1-03
2000 a.u.
NL1-02
500 1000 1500 2000 2500 3000
Raman schift (cm-1)

Raman Spectral Maturity Tracers (Quirico et al., 2005 method)

COAL	ω_D (cm^{-1})	ω_G (cm^{-1})	I_D / I_G	FWHM-D (cm^{-1})	FWHM-G (cm^{-1})	$\frac{A_D}{A_D+A_G}$
A2	1346	1570	0.819	273.78	114.70	0.673
A3	1348	1571	0.669	227.88	110.76	0.582
CS2	1348	1571	0.770	241.87	125.06	0.609
USA1	1316	1602	1.206	152.10	43.29	0.797
TR1	1307	1602	1.140	168.10	47.64	0.799
SU1	1292	1586	2.021	104.52	54.41	0.797
GB3	1340	1587	1.143	243.14	84.90	0.799
GB1	1349	1602	1.166	259.48	151.55	0.721
NL1	--	--	--	--	--	--

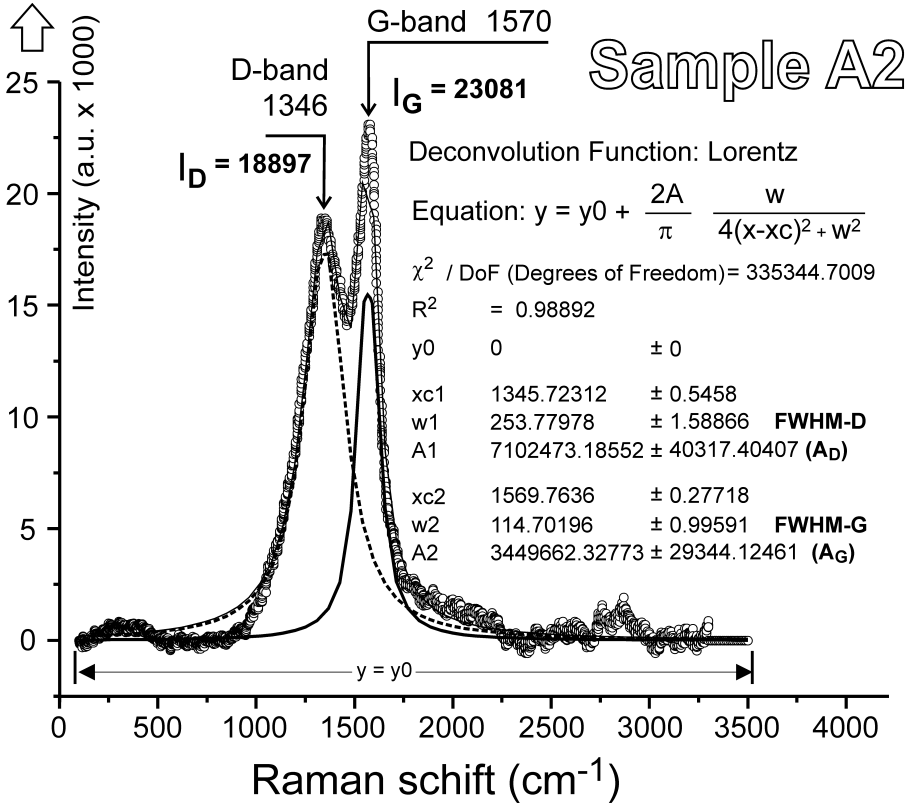

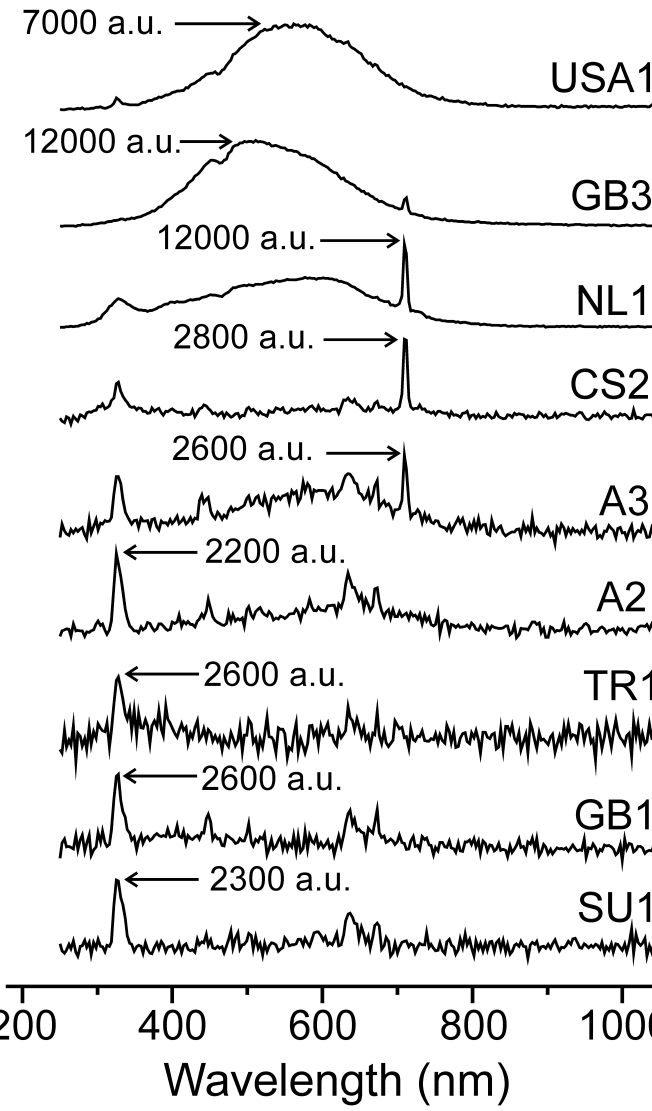
7000 a.u.
USA1
12000 a.u.
GB3
12000 a.u.
NL1
2800 a.u.
CS2
2600 a.u.
A3
2200 a.u.
A2
2600 a.u.
TR1
2600 a.u.
GB1
2300 a.u.
SU1
200
400
600
800
1000
Wavelength (nm)

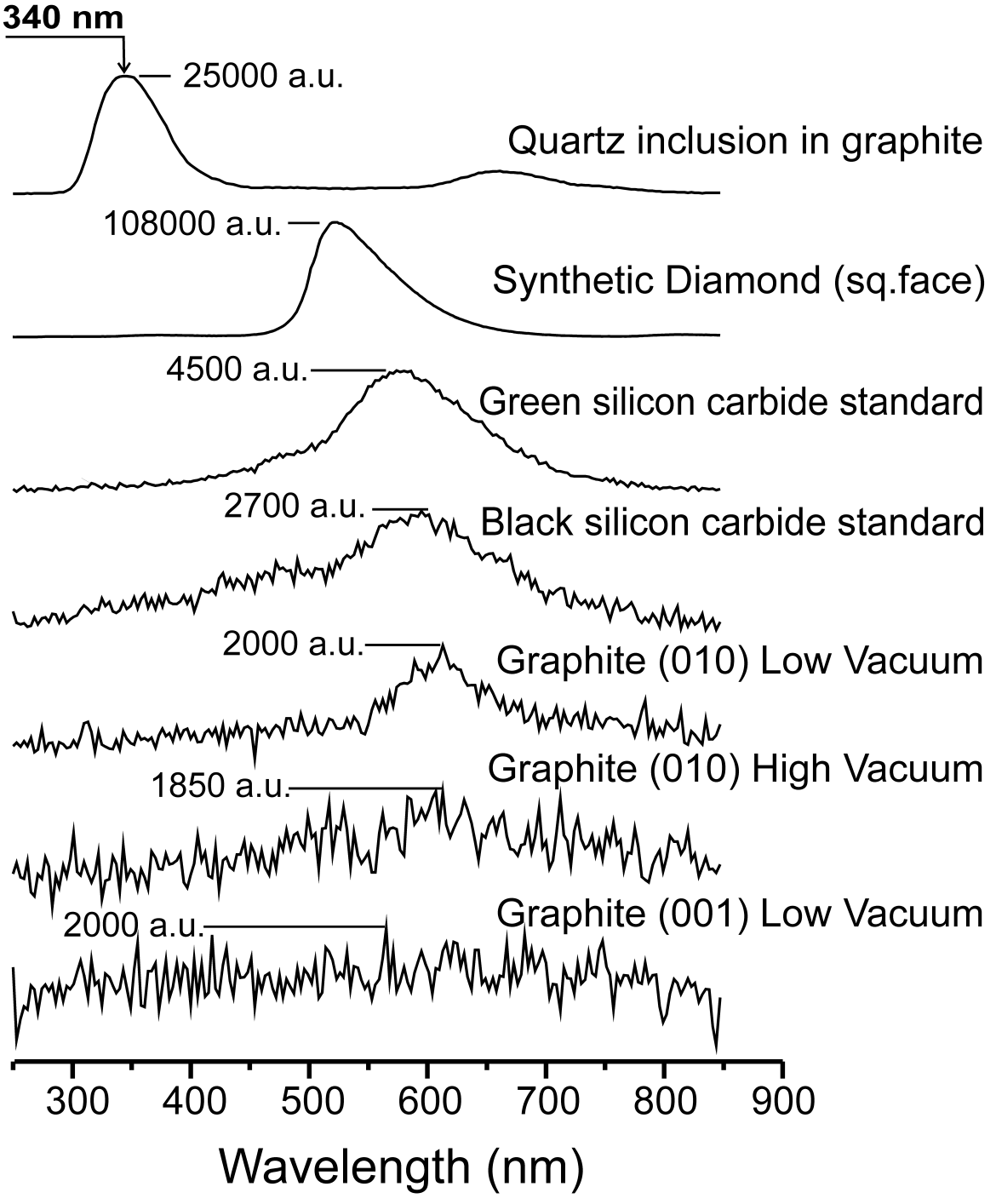
340 nm
25000 a.u.
Quartz inclusion in graphite
108000 a.u.
Synthetic Diamond (sq.face)
4500 a.u.
Green silicon carbide standard
2700 a.u.
Black silicon carbide standard
2000 a.u.
Graphite (010) Low Vacuum
Graphite (010) High Vacuum
1850 a.u.
Graphite (001) Low Vacuum
2000 a.u.
300
400
500
600
700
800
900
Wavelength (nm)